AGU PUBLICATIONS

JGR

Journal of Geophysical Research: Oceans

RESEARCH ARTICLE
10.1002/2016JC012374

The Angola Current: Flow and hydrographic characteristics as observed at 11°S

R. Kopte[1], P. Brandt[1,2], M. Dengler[1], P. C. M. Tchipalanga[3], M. Macuéria[3], and M. Ostrowski[4]

[1]GEOMAR Helmholtz Centre for Ocean Reseach Kiel, Kiel, Germany, [2]Christian-Albrechts-Universität zu Kiel, Kiel, Germany, [3]Instituto Nacional de Investigacaõ Pesqueira (INIP), Luanda, Angola, [4]Institute for Marine Research (IMR), Bergen, Norway

Key Points:
- Moored observations of the Angola Current at 11°S
- Semiannual cycle of current strength and stratification
- Assessment of ocean reanalysis' performance in terms of current strength and thermal structure off Angola

Correspondence to:
R. Kopte,
rkopte@geomar.de

Citation:
Kopte, R., P. Brandt, M. Dengler, P. C. M. Tchipalanga, M. Macuéria, and M. Ostrowski (2017), The Angola Current: Flow and hydrographic characteristics as observed at 11°S, *J. Geophys. Res. Oceans*, *122*, 1177–1189, doi:10.1002/2016JC012374.

Received 27 SEP 2016
Accepted 4 JAN 2017
Accepted article online 7 JAN 2017
Published online 15 FEB 2017

Abstract The eastern boundary circulation off the coast of Angola has been described only sparsely to date, although it is a key element in the understanding of the highly productive tropical marine ecosystem off Angola. Here, we report for the first time direct velocity observations of the Angola Current (AC) at ~11°S collected between July 2013 and October 2015 in the depth range from 45 to 450 m. The measurements reveal an alongshore flow that is dominated by intraseasonal to seasonal variability with periodically alternating southward and northward velocities in the range of ±40 cm/s. During the observation period, a weak southward mean flow of 5–8 cm/s at 50 m depth is observed, with the southward current extending down to about 200 m depth. Corresponding mean southward transport of the AC is estimated to be 0.32 ± 0.046 Sv. An extensive set of hydrographic measurements is used to investigate the thermal structure and seasonality in the hydrography of the eastern boundary circulation. Within the depth range of the AC, the superposition of annual and semiannual harmonics explains a significant part of the total variability, although salinity in the near surface layer appears to be also impacted by year-to-year variability and/or short-term freshening events. In the central water layer, temperature and salinity on isopycnals vary only weakly on seasonal to annual time scales. The available data set is further used to evaluate different reanalysis products particularly emphasizing the ocean's role in coupled climate model SST biases in the Eastern Tropical Atlantic.

1. Introduction

North of the Benguela upwelling region—one of the world's four major Eastern Boundary Upwelling Systems (Benguela-Canaries-Humboldt-California, e.g., *Carr and Kearns* [2003]; *Chavez and Messié* [2009])—the tropical Angolan system represents another highly-productive ecosystem [*Ostrowski et al.*, 2009]. Located en route from the equatorial Atlantic, the region off Angola thereby serves as the gateway for communicating equatorial oceanic variability to the northern Benguela, mainly via poleward propagation of coastally trapped waves (CTWs). At about 16°S the Angola-Benguela Front (ABF) represents a sharp, yet highly-variable thermal front, separating at the surface tropical, oligotrophic waters in the north from cold waters, enriched in nutrients by upwelling in the south [*Mohrholz et al.*, 2008]. Fluctuations in position and strength of the frontal system range from subseasonal [*Kostianoy and Lutjeharms*, 1999; *Mohrholz et al.*, 2001], via annual [*Meeuwis and Lutjeharms*, 1990], to interannual time scales. The latter are often associated with severe warm events during austral summer being referred to as Benguela Niños [*Shannon et al.*, 1986]. Most of the observed interannual variability is induced by wave response via equatorial Kelvin waves and CTWs to the remote equatorial forcing [*Bachèlery et al.*, 2016; *Florenchie et al.*, 2003; *Lübbecke et al.*, 2010; *Rouault et al.*, 2007], yet modulated by local wind forcing [*Bachèlery et al.*, 2016; *Richter et al.*, 2010]. Anomalous oceanic conditions in the region have been found to substantially impact precipitation variability over adjacent countries [*Rouault et al.*, 2003] as well as the marine ecosystem and local fisheries [*Gammelsrød et al.*, 1998].

Within the tropical Angolan system, the Angola Current (AC) is one key element in the poleward advection of warm tropical waters. It is suggested to be fed by eastward equatorial currents, namely the Equatorial Undercurrent, the South Equatorial Undercurrent, and the South Equatorial Counter Current, as well as the Gabon Current (Figure 1a) [*Peterson and Stramma*, 1991; *Rouault et al.*, 2007; *Wacongne and Piton*, 1992]. Its variability in strength is found to be partly controlled by the passage of CTWs [*Ostrowski et al.*, 2009; *Rouault*, 2012]. The large-scale properties of the AC have been described exclusively based on synoptic

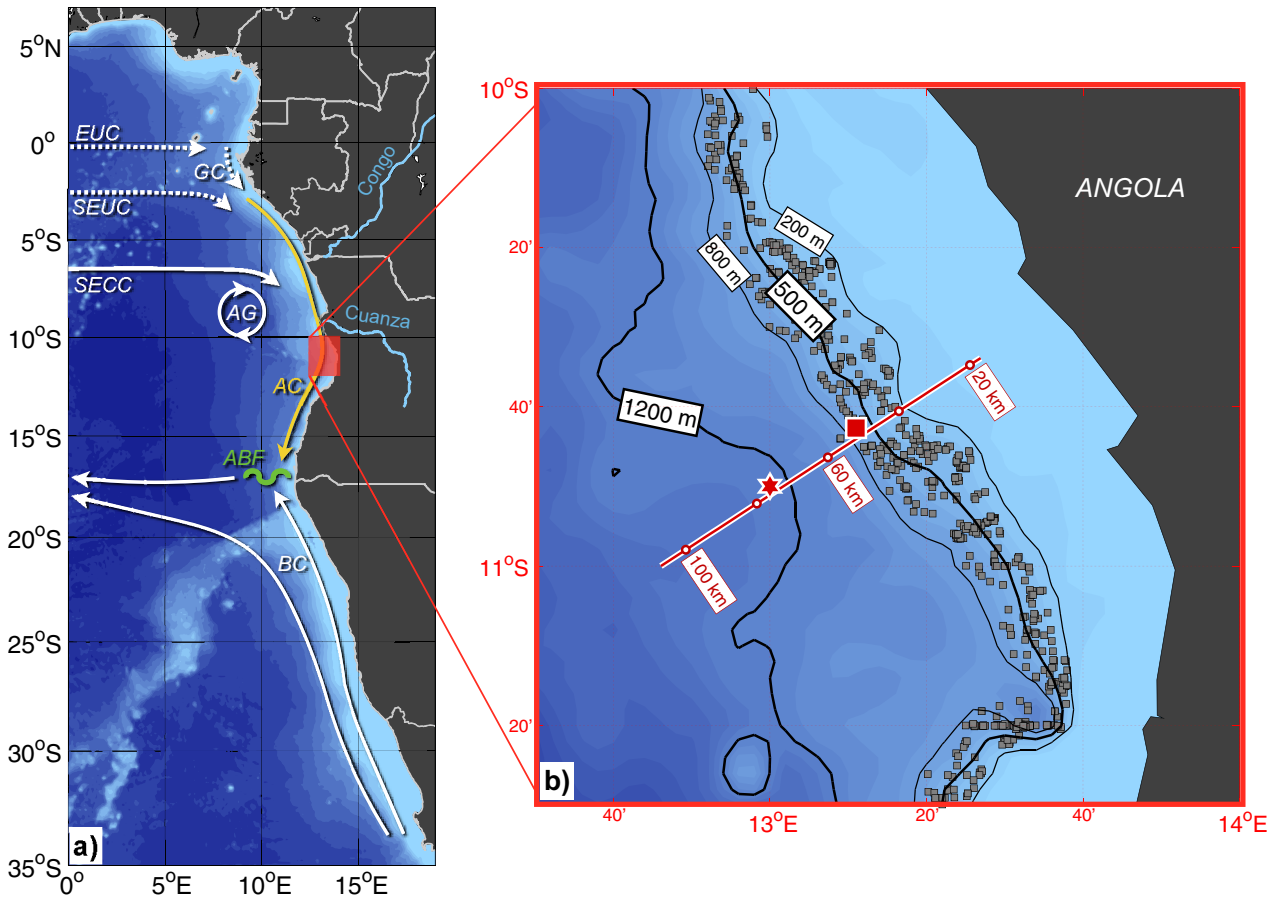

Figure 1. (a) Schematic circulation in the Southeast Atlantic Ocean (modified from *Rouault et al.* [2007]). Main features are the Equatorial Undercurrent (EUC), South Equatorial Undercurrent (SEUC), South Equatorial Counter Current (SECC), Gabon Current (GC), Angola Gyre (AG), Angola Current (AC), and Benguela Current (BC). The mean position of the Angola-Benguela Front (ABF) is indicated. (b) Enlargement of the study area indicating the positions of ADCP mooring (red star) and ADCP shield (red square) as well as the ~11°S section (solid red line, white dots represent along-section distance to the coast (km)). Gray dots represent positions of all hydrographic profiles used in this study. Bathymetry is extracted from ETOPO2, with black lines representing individual isobaths.

measurements so far. Subsurface southward geostrophic velocities exceeding 50 cm/s were reported along the Angolan coast between 9°S and 16°S during a hydrographic survey in 1968 with southward velocities extending from the surface down to 250–300 m depth [*Moroshkin et al.*, 1970]. Current velocities were measured at 12°S on four occasions between September 1970 and July 1971 [*Dias*, 1983a,1983b]. In March 1971 southward flow was found to be stronger compared to July 1971: 50 cm/s versus 42 cm/s at the surface, 70 cm/s versus 33 cm/s at 100 m depth, respectively. Southward transports above 400 m depth were calculated in the range of 1.2–3.7 Sv between September 1970 and July 1971 [*Dias*, 1983a]. However, results of an inverse model study making use of WOCE line A13, which was sampled during a major Benguela Niño event between January and March 1995 [*Gammelsrød et al.*, 1998], suggest a southward transport of 11 Sv of the AC within surface and thermocline layers [*Mercier et al.*, 2003]. During a survey in April 1999 a secondary, offshore branch of southward subsurface flow was identified in shipboard velocity data separated from the coastal branch [*Mohrholz et al.*, 2001]. Both pathways were characterized by southward velocities of about 40 cm/s below the surface. However, below 150 m depth northward currents of 15–20 cm/s were observed in the coastal branch. Based on the available synoptic snapshots, the general perception of the AC is that of a continuous poleward current which is stronger in austral summer and weaker in austral winter. During Benguela Niños the AC appears to be a major agent in advecting warm tropical waters poleward into the northern Benguela [*Gammelsrød et al.*, 1998; *Rouault et al.*, 2007].

Along with the eastern equatorial Atlantic, the Southeast Atlantic Ocean and particularly the ABF region is subject to the strongest sea surface temperature (SST) biases seen in many state-of-the-art coupled climate simulations [*Davey et al.*, 2002; *Richter et al.*, 2014]. A common indicator of the bias is an erroneous tilt of

the equatorial thermocline associated with reduced zonal winds, nonetheless the origin of the bias remains highly controversial. Mainly deficiencies in the atmosphere models have been proposed as source of the bias, such as a misrepresentation of convection over the Amazon and West Africa [*Richter and Xie*, 2008], erroneous localized Bjerknes feedback in the Gulf of Guinea [*Patricola et al*., 2012], or errors in radiation and low clouds over the upwelling regions [*Huang et al*., 2007]. It could be shown that a reduction of the bias is possible particularly by improving the near-coastal winds when enhancing simultaneously the horizontal and vertical resolution of the atmospheric model in coupled simulations [*Harlaß et al*., 2015]. However, also systematic errors in ocean models potentially contribute to the bias problem [*Grodsky et al*., 2012; *Large and Danabasoglu*, 2006; *Xu et al*., 2014]. In particular, the representation of the AC and the tropical Angolan system in ocean models as well as reanalysis products have been identified to cause biases in the Southeast Atlantic [*Xu et al*., 2014]. First, based on comparisons with a reference reanalysis product, usually an overshooting of the AC is observed near the ABF causing a southward shift of the front and thus introducing a strong warm SST bias. Second, ocean models tend to have difficulties to simulate the sharp thermocline off Angola, which results in too-warm subsurface temperatures being advected southward into the northern Benguela by a deep continuation of the AC and subsequently upwelled to manifest in too-warm SSTs. In this context the need for in situ ocean observations to validate both AC strength and thermal structure off Angola in ocean models and reanalysis data has been emphasized.

For the first time, moored observations of the boundary circulation at ∼11°S off the coast of Angola are available between July 2013 and October 2015. They give insight into the mean state and variability of the AC. Furthermore, based on an extensive set of hydrographic measurements from shipboard and autonomous glider measurements covering the period from 1968 to 2015, the seasonality of hydrographic properties at the eastern boundary off Angola is investigated. Finally, the observed thermal structure and alongshore velocities are used to qualitatively assess the performance of various reanalysis products in the boundary current system off Angola.

2. Data and Methods

2.1. Mooring Data

Multiyear velocity measurements were obtained by a mooring array deployed at ∼11°S off the coast of Angola for the period from July 2013 to October 2015 (Figure 1b). A bottom shield equipped with a 75 kHz Teledyne RDI's Workhorse Long Ranger ADCP, which was sampling every 2.5 min, was located at 500 m water depth (13°11.0′E, 10°42.7′S, 53 km offshore, red square in Figure 1b), accompanied by a mooring sitting on the 1200 m isobath (13°00′E, 10°50.0′S, 77 km offshore, red star in Figure 1b) with another 75 kHz Long Ranger ADCP being installed at 500 m depth and sampling every hour. Both upward-looking instruments measured the current speed in the overlying water-column up to about 45 m below the sea surface. During data processing, a 40 h low pass filter was applied to hourly-interpolated current data to eliminate tidal currents followed by a subsampling of the detided data to 12 hourly resolution. The local orientation of the shelf break (−34°) was used for the calculation of the alongshore component of the flow.

Additionally, temperature time series were recorded at the instrument depths.

2.2. Shipboard and Autonomous Glider Data

Since 1983, an extensive oceanographic data set from repeated ship surveys carried out in Angolan territorial waters has been acquired within the EAF-Nansen program executed by the Food and Agriculture Organization of the United Nations (FAO) and funded by Norwegian Agency for Development Cooperation (NORAD). Semiannual cruises (austral summer versus austral winter) have been carried out by R/V Dr. Fridtjof Nansen on a regular basis since 1995, collecting data to estimate the abundance and map the distribution of the main commercially important fish species, to perform biogeochemical measurements and to collect hydrographic data. Since 2005, shipboard ADCP measurements from a 150 kHz Teledyne RDI Ocean Surveyor are available.

Recently, shipboard CTD measurements and upper ocean velocities recorded by a 75 kHz Teledyne RDI Ocean Surveyor were collected along a section perpendicular to the topography (red line in Figure 1b, hereinafter referred to as "∼11°S section") during R/V Meteor cruises M98 in July 2013 and M120 in October 2015, when the moorings described in section 2.1 were deployed and serviced, respectively.

2.2.1. Shipboard Current Measurements

From the two data sets described above, we use a total number of 13 upper ocean velocity sections. Eleven sections were acquired within the EAF-Nansen program on a monitoring line perpendicular to the topography near 12°S (sampling times: March 2007, March 2008, June 2008, March 2009, June 2009, March 2010, July 2010, March 2011, August 2011, February 2014, July 2014), another two stem from samplings of the ~11°S section by R/V Meteor (sampling times: July 2013, October 2015).

2.2.2. Hydrographic Measurements

A total number of 707 temperature/salinity profiles sampled on the Angolan shelf break within 200 and 800 m water depth between 11.5°S and 10°S is used (grey dots in Figure 1b), incorporating 644 profiles obtained within the EAF-Nansen program between 1991 and 2015, as well as eight profiles collected during the two R/V Meteor cruises in 2013 and 2015. The majority of these profiles were obtained during March/April, July/August, and October. In particular these data sets do not provide hydrographic information for the December/January period. In order to improve the seasonal coverage, additional historic data were incorporated into the analysis: 52 temperature/salinity profiles were extracted from the input data set for the MIMOC climatology [*Schmidtko et al*., 2013], originating mainly from the 1980s but as early as 1968; one profile was taken during R/V Poseidon cruise 250 (April 1999, *Mohrholz et al*. [2001]), one during R/V Meteor cruise 48/3 (September 2000, *Mohrholz et al*. [2008]), and another one during R/V Maria S. Merian cruise 18/4 (August 2011, *Mohrholz et al*. [2014]). Note that the extended data set does contain three profiles for December/January; however, these profiles are limited to the upper 200–450 m depth.

Supplementary to the shipboard hydrographic measurements, we include data from an autonomous Slocum glider (Teledyne Webb Research) that was deployed in the study area from 31 October 2015 to 27 November 2015 (Glider IFM03, deployment-ID: ifm03_depl12). Glider data were internally recorded as time series along the flight path, while for the analysis the data are interpolated onto a regular pressure grid of 1-dbar resolution (see also *Thomsen et al*. [2016] for further details on data processing). During its deployment, the glider sampled along the ~11°S section, travelling onshore and offshore five times each thereby acquiring 364 CTD profiles within the section segment between 200 and 800 m water depth.

2.3. Auxiliary Data Sets

As the moored ADCP measurements do not provide near-surface velocity observations, we use the delayed-time "all-sat-merged" data set of absolute geostrophic velocities derived from absolute dynamic topography, produced by Ssalto/Duacs and distributed by AVISO, with support from CNES (Version 2014, http://www.aviso.altimetry.fr/duac/). This multimission product is mapped on a 0.25 × 0.25° grid and provided on daily resolution. However, note that the mapping algorithm takes into account data from a latitude-dependent multiday window using Gauss-Markov weighting (~12 days at 11°S, for further details on the mapping procedure see *Pujol et al*. [2016]). Only data from the closest grid point to the mooring positions and corresponding to the mooring deployment period are considered here. A similar extraction is done for sea level anomaly (SLA) data.

For sea surface temperature (SST), we make use of the "Microwave plus Infrared (MW_IR) Optimally Interpolated SST" product provided by Remote Sensing Systems (www.remss.com). This data set combines through-cloud capabilities of microwave sensors (TMI, AMSR-E, AMSR2, WindSat) with high spatial resolution of infrared SST data (Terra MODIS, Aqua MODIS), yielding 9 km horizontal resolution. Using a diurnal model, SST values are corrected to create representative 12:00 LT temperatures (www.remss.com). Daily values from 2006 to 2015, spatially averaged over the Angolan shelf break within 200 and 800 m water depth between 11.5°S and 10°S are used here.

2.4. AC Transport Estimation

In order to obtain an estimate of the AC transport, a time series of the two-dimensional flow field (as function of distance from coast and depth) is required. Our approach is to apply an inter/extrapolation scheme to the moored velocity time series described in section 2.1. The inter/extrapolation is based on the variability patterns (Figure 2) of 13 shipboard velocity sections collected between ~11°S and 12°S as described in section 2.2.1. As the topographic slope is very similar for all these sections, we choose a reference bathymetry representing the shelf break at the ~11°S section and rearrange alongshore velocity profiles from other sections with respect to depth. Subsequently, the rearranged sections are interpolated on a reference grid. The resulting sections are assumed to give the best estimate of variability contained in the alongshore flow

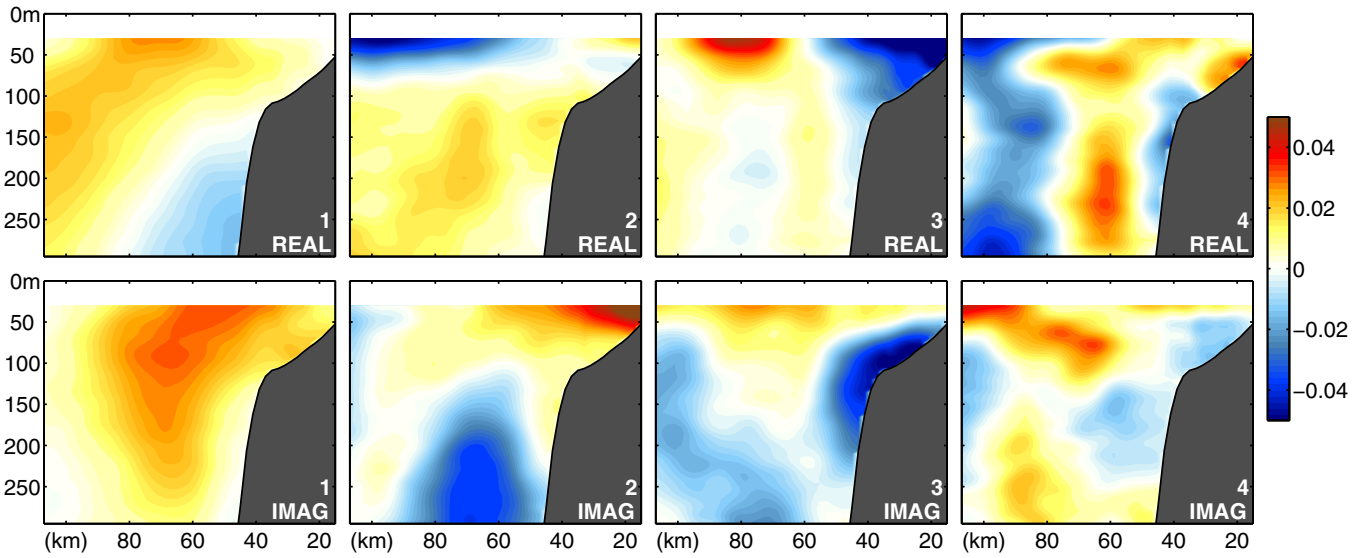

Figure 2. HEOF patterns (dimensionless, sign is arbitrary) as calculated from 13 ship sections. Column 1–4 corresponds to HEOF 1–4 with each HEOF consisting of two patterns. Top and bottom plots correspond to the patterns from the real and imaginary HEOF, respectively.

field, although a bias cannot be ruled out considering the sampling times with regard to the seasonal cycle (mainly austral summer and austral winter).

Note that some of the ship sections were limited in their offshore and/or vertical extent. Therefore, before deriving variability patterns, any gaps in these sections were closed by regressing their valid data on the first 20 variability patterns calculated from corresponding section data from the high-resolution OGCM INALT01 [*Durgadoo et al*., 2013], and subsequently extrapolating the respective ship sections to full offshore and vertical extent.

A Hilbert transformation is applied to the alongshore velocity fields of the ship sections [*Barnett*, 1983; *Brandt et al*., 2014]. Hilbert EOFs (HEOFs), containing real and imaginary patterns, are obtained by applying empirical orthogonal function (EOF) analysis to the Hilbert transform of alongshore velocity.

The summed up contribution of eight real spatial patterns, which were derived from the first four complex EOFs (Figure 2), explains 96% of the variability contained in the ship sections. These eight real patterns are then regressed on the mooring time series of alongshore velocity. Regressed fields are summed up and the resulting time series of the two-dimensional velocity field is integrated in the limits of 15–90 km offshore and 30–200 m depth to obtain a transport time series. The method is validated by reconstructing the ship sections using the variability patterns (in varying numbers) and the velocity profiles from the ship sections corresponding to the mooring locations. Then the observed AC transport from the ship sections can be compared to the AC transport estimated from the reconstructed sections (Figure 3). A balanced compromise has to be found between simplicity and explained variance. Here we decide on using the first four HEOFs (or eight real spatial patterns) for the reconstruction, as they give the lowest RMS between observed and reconstructed AC transport.

2.5. Seasonality of Hydrographic Properties

The seasonality of potential temperature and salinity within the current regime is investigated using hydrographic profiles collected within the EAF-Nansen program, and various cruises with R/V Meteor, R/V Maria S. Merian, and R/V Poseidon, supplemented by autonomous glider data as well as historical data (see section 2.2.2). For each cruise/glider section, a mean potential temperature and salinity profile is derived from all measurements taken between 200 and 800 m water depth along the continental slope near 11°S. Subsequently, these mean profiles are sorted with respect to the calendar year and are interpolated using a depth-time Gaussian weighting (vertical/temporal half width scale of 5 m/25 days and cutoff scales of 10 m/300 days) to construct a mean seasonal distribution. Note that the chosen interpolation scales leave the amplitude of an annual harmonic almost unaffected, whereas the amplitude of a semiannual harmonic

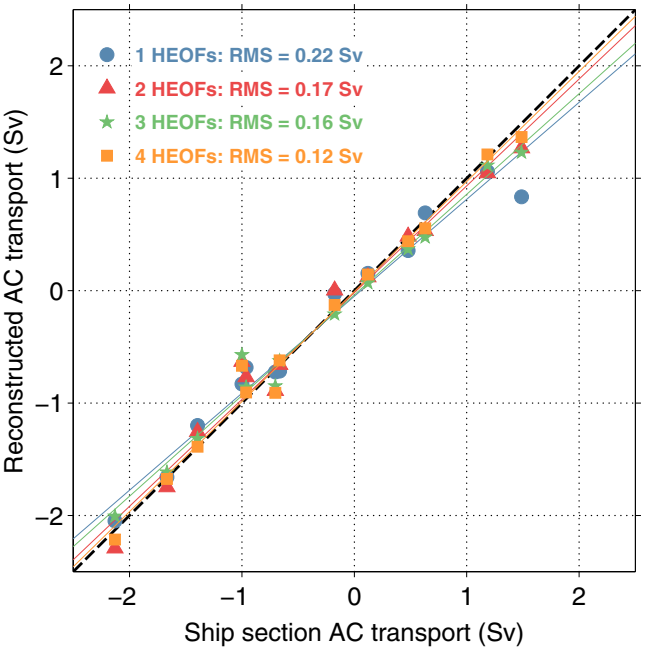

Figure 3. Observed versus reconstructed AC transport obtained by regressing various numbers of real pattern derived from HEOF analysis (corresponding to Figure 2) on the shipboard velocity profiles measured at the mooring positions. Solid lines are linear regressions with RMS values given in the legend.

would be reduced by about 20%. The contribution of the annual cycle to the seasonality is investigated by fitting an annual harmonic to the potential temperature and salinity distribution at each depth level. The effect of potential long-term trends on the seasonality has been evaluated by removing linear trends at each depth level before the interpolation. Trends are strongest but also most uncertain in the near surface layers and have been found to be smaller than 0.4°C per decade for temperature and 0.15 per decade for salinity. However, removing these trends does not alter significantly the seasonal distribution and particularly the amplitudes of the annual harmonic. Thus, as robust trends are difficult to assess from the available data distribution, particularly when including historical data acquired as early as 1969, and their effect on the seasonality appears to be negligible, we decide on using the nondetrended data set for the analysis of the seasonality.

3. Results

3.1. Alongshore Flow and Transport of the AC

The alongshore flow observed by the moored ADCPs described in section 2.1 at ~11°S is dominated by alternating periods of southward and northward velocities that can last for a couple of months with superimposed high-frequency velocity pulses (Figures 4a and 4c). Stronger velocities were recorded by the onshore ADCP (located 53 km off the coast), with maximum velocities exceeding ±40 cm/s. Considering vertical structure, the offshore ADCP (located 77 km off the coast) measured more depth-independent current profiles. The alongshore component of surface geostrophic velocities from AVISO is found to be coherent with the top-most observations of the ADCPs at about 45 m depth during most of the observation period (significantly correlated at the 95%-level with $r = 0.49$ for the onshore ADCP and $r = 0.44$ for the offshore ADCP). The mean profile of alongshore velocity from the onshore ADCP, which was derived by first removing the mean seasonal cycle to avoid a seasonal bias due to the record length of 2.5 years, indicates southward flow in the upper 210 m with maximum southward velocities of 8 cm/s at 50 m depth (Figure 4b). Offshore, the mean southward flow extends down to about 160 m depth with maximum velocities of 5 cm/s also at about 50 m depth (Figure 4d). Mean southward surface geostrophic velocities are found to be 5 cm/s at the onshore and 3 cm/s at the offshore mooring position.

The mean alongshore velocity across the ~11°S section (Figure 5a) is obtained from time-averaging the time series of the reconstructed two-dimensional velocity field, which was calculated using both the variability patterns from the shipboard velocity sections and the moored velocity time series (section 2.4). The southward maximum of alongshore velocity is located in 50–60 m depth at a distance from the coast close to that of the onshore ADCP, whereas the offshore ADCP appears to monitor the offshore termination of the mean southward flow of the boundary current. Based on the mean flow pattern, a box extending from 15 to 90 km offshore and 30 to 200 m depth is chosen representing the area occupied by the AC. The resulting AC volume transport time series is dominated by submonthly to intraseasonal variability, ranging from 2.2 Sv southward to 1.2 Sv northward (Figure 5b). For the observational period, a mean southward transport of 0.32 Sv (standard deviation: 0.59 Sv) is derived. Accounting for the top 30 m by extrapolating moored velocities linearly to surface geostrophic velocities before reconstructing the flow field, yields 0.54 Sv

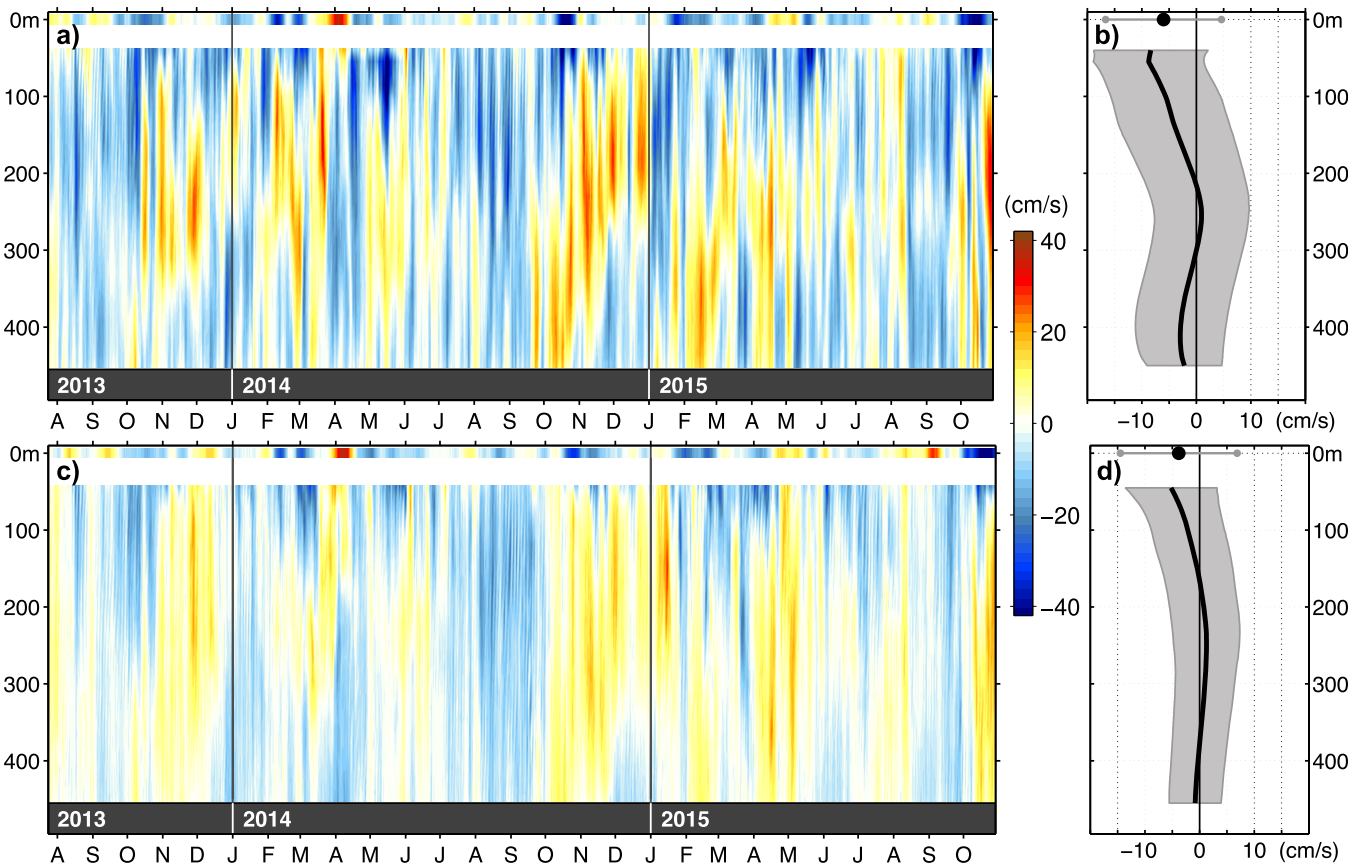

Figure 4. Time series of alongshore velocity (−34°) as measured by (a) the onshore ADCP in the bottom shield and (c) the offshore ADCP in the mooring. Positive values indicate northward and negative values indicate southward flow. Corresponding mean alongshore velocity profiles (thick black lines) and standard deviations (shaded areas) are shown in (b) and (d), respectively. At the surface corresponding AVISO geostrophic alongshore velocities are plotted.

(standard deviation: 0.88 Sv) for the 0–200 m depth range. Four individual transport estimates from available ship sections during the mooring period agree with the reconstructed time series. The inherent submonthly to intraseasonal fluctuations hamper a clear identification of semiannual and annual flow components (Figure 5b). However, the semiannual component with amplitude of 0.20 Sv was found slightly

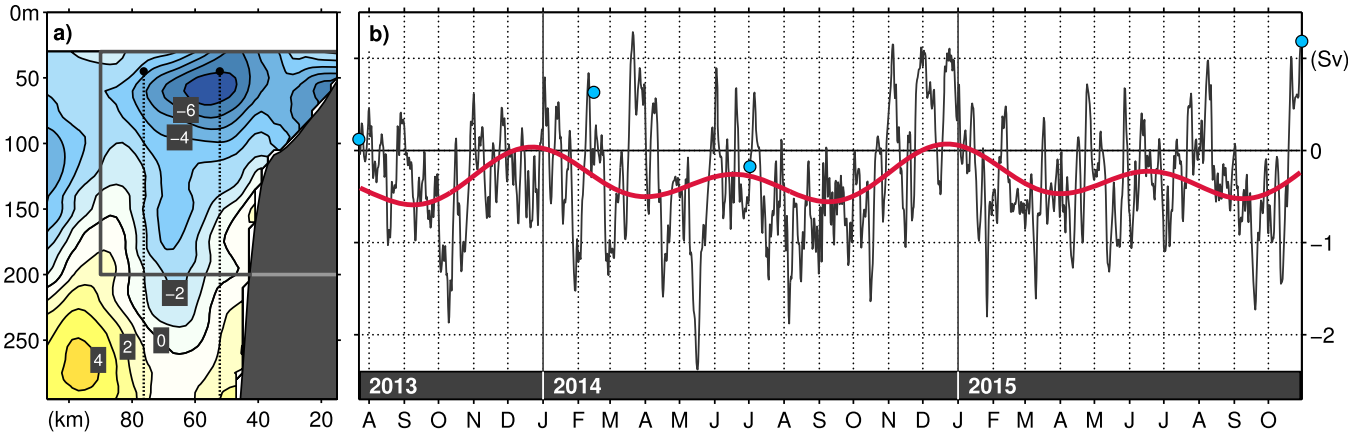

Figure 5. (a) Mean alongshore velocity field (cm/s) based on the reconstruction of the 3-D flow field using mooring data and eight real pattern from the first four HEOFs. Positive values indicate northward and negative values indicate southward flow. (b) Transport time series (black line) obtained by integrating the alongshore velocity from 30 to 200 m depth and from 15 to 90 km offshore (see grey box in Figure 5a). Red line displays sum of semiannual and annual harmonic. Blue dots indicate individual transport estimates based on shipboard velocity sections obtained during the mooring period.

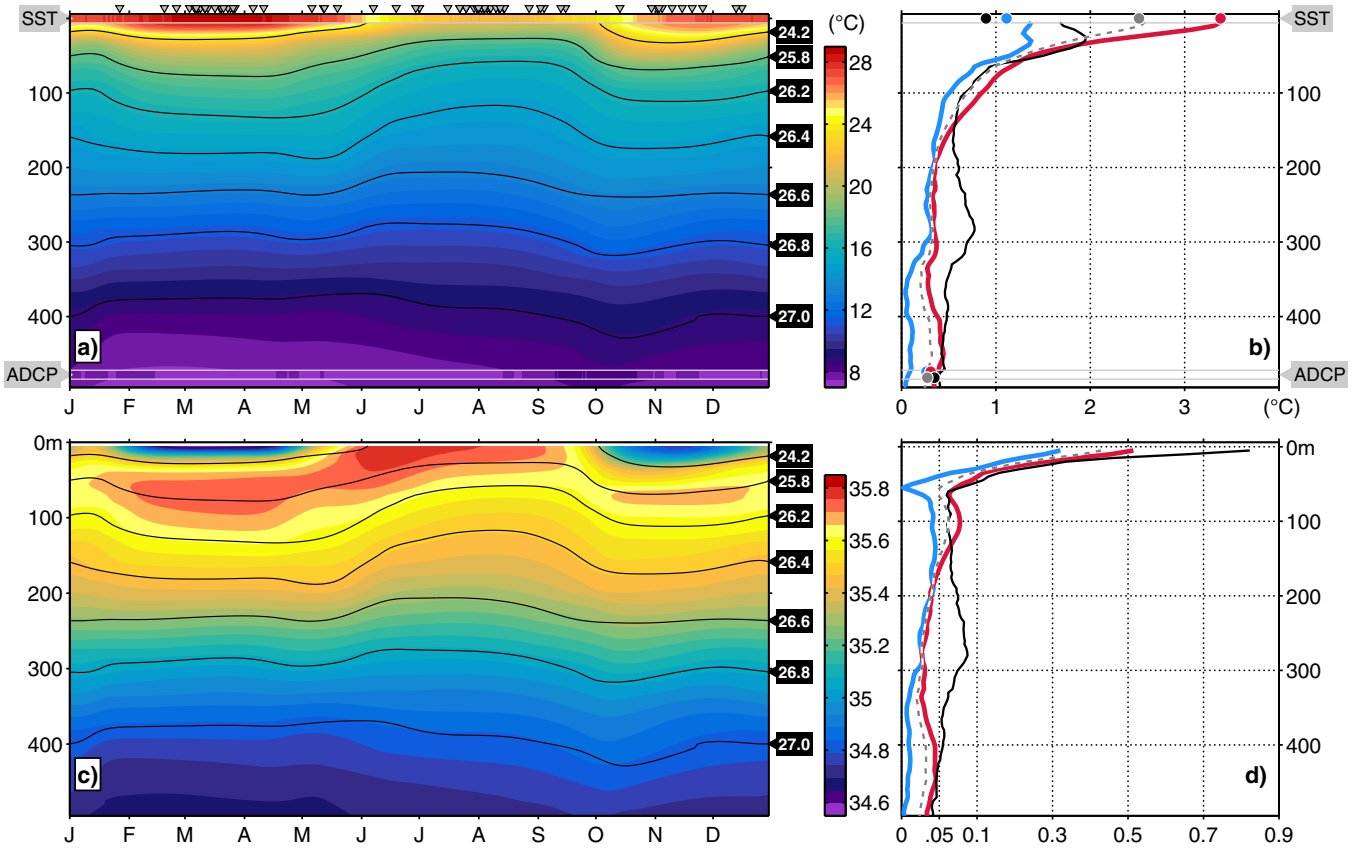

Figure 6. Seasonal distribution of (a) potential temperature and (c) salinity derived from available hydrographic measurements in the study area. Sampling times of used profiles relative to the calendar year are indicated by grey triangles at the top of Figure 6a. In Figure 6a also the seasonal cycles of SST and of potential temperature as recorded by the ADCPs are indicated. Black lines represent isopycnals. On the right, red and blue lines depict amplitudes of the annual and semiannual harmonics, respectively, as fitted to the seasonal distribution of (b) potential temperature and (d) salinity. Solid black lines show the RMS of the residuals derived by subtracting annual and semiannual harmonics from the individual profiles, whereas dashed gray lines show the RMS of the sum of annual and semiannual harmonics.

stronger than the annual component with amplitude of 0.16 Sv. The superposition of both harmonics suggests March/April and September/October as the periods of maximum southward transport.

3.2. Seasonality of Hydrographic Properties in the Current Regime

The seasonality of potential temperature and salinity at the continental slope at ~11°S reflects mainly the major seasons of down and upwelling. Warm/fresh waters occupy the mixed layer during downwelling in March, whereas cold/saline waters prevail during upwelling in August (Figures 6a and 6c). Although December/January are only sparsely sampled and thus are strongly dependent on the chosen interpolation scales, the secondary upwelling during this period is indicated by upward bending isopycnals within the upper 200 m, thereby separating the major downwelling season in March from the secondary downwelling in October/November. By suggesting no more than a weak cooling in December/January, the main periods of down and upwelling are also indicated in the seasonal cycle of SST. At depth, the seasonal distribution of potential temperature derived from the shipboard hydrographic data agrees with the seasonal cycle as recorded by the temperature sensors of the moored ADCPs both in amplitude and evolution over the year (Figure 6a), suggesting that the observing period from 2013 to 2015 can be considered as a period with a rather regular seasonal cycle. The individual contributions of both semiannual and annual cycles are inferred by fitting corresponding harmonics to the seasonal distributions of potential temperature and salinity (Figures 6b and 6d, respectively), as well as to the seasonal cycles of SST and temperature as recorded by the ADCP. As noted earlier, the amplitude of the semiannual cycle in the interpolated fields is likely to be reduced by about 20% due to the chosen temporal interpolation scales. However, in agreement with SST seasonality, the seasonality in the near-surface layers appears to be dominated by the annual cycle. The annual harmonic amplitude of potential temperature is found to be larger than 3°C for potential

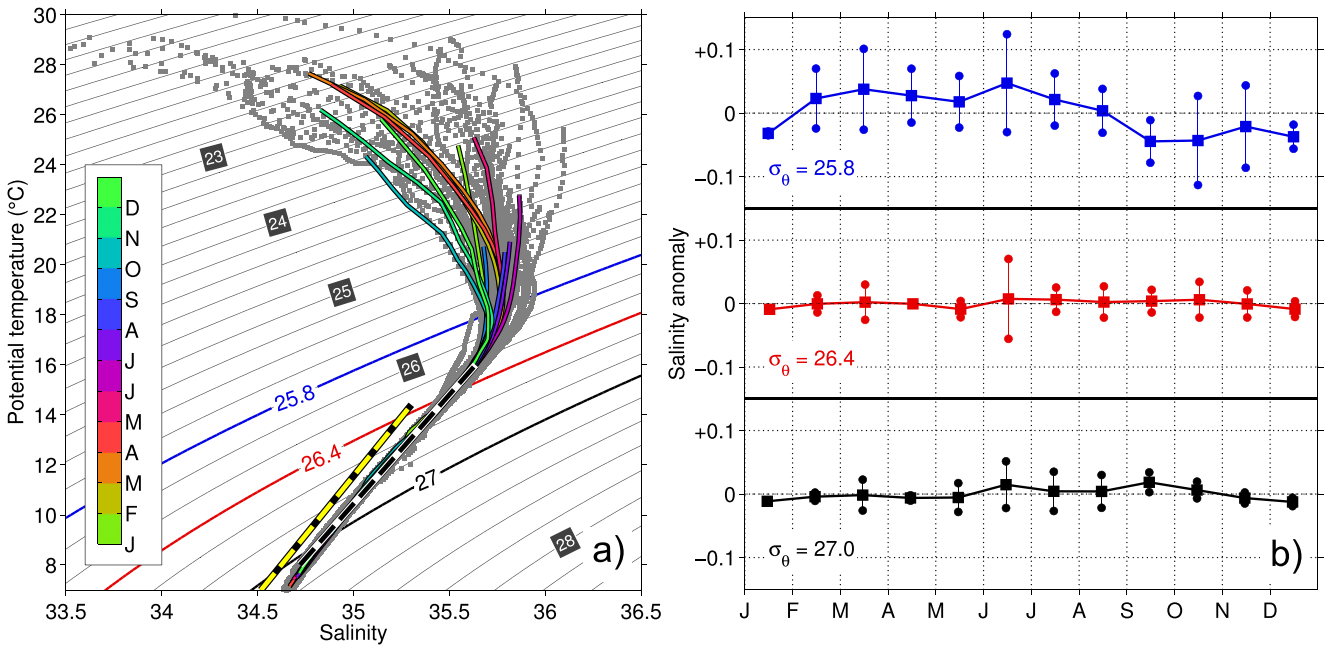

Figure 7. (a) θ/S diagram of all available hydrographic measurements (grey dots). Colored lines show monthly mean characteristics derived from the interpolated seasonal distribution. Black-dashed and yellow-dashed lines correspond to the SACW and ESACW characteristics, respectively, as defined in *Mohrholz et al.* [2008]. (b) Mean seasonal cycle of salinity anomalies on selected isopycnals. Error bars indicate the corresponding monthly RMS of the residuals derived by subtracting the mean seasonal cycle from individual profiles.

temperature, and that of salinity about 0.5. Corresponding semiannual amplitudes do not exceed 1.4°C for potential temperature and 0.3 for salinity. Within the depth range of the AC (50–200 m depth), the dominance of the annual cycle decreases with depth and amplitudes of semiannual and annual harmonic approach similar levels. Below 200 m depth, there is only weak seasonality with both semiannual and annual amplitudes smaller than 0.5°C for potential temperature and 0.05 for salinity. Here, semiannual amplitudes are likely being masked by the interpolation, as there is no deep data available for the December/January period. The RMS of the residuals obtained by subtracting the semiannual and annual harmonics from the individual potential temperature and salinity profiles gives a measure of the relative contribution of the derived seasonality to the total variability contained in the hydrographic data and can be compared to the RMS of the sum of semiannual and annual harmonic (Figure 6b, d). For potential temperature, the RMS of the residuals is considerably smaller than the RMS of semiannual and annual harmonic in the near-surface layers, while it is larger for near-surface salinity. Whether intraseasonal or interannual variability dominates the residual fluctuations cannot be resolved with the available hydrographic data. Though, the low-pass-filtered SST time series (cutoff period of 365 days, annual, and semiannual harmonic removed prior filtering) suggests a RMS of 0.46°C for interannual fluctuations. Correspondingly, for intraseasonal fluctuations the high-pass-filtered version of the SST time series (cutoff period of 365 days) shows a RMS value of 0.66°C. This indicates slightly higher importance of intraseasonal variability at least for temperature in the near-surface layer. Near the core depth of the AC, the RMS of potential temperature and salinity residuals are found to be in the same range or only slightly larger than the corresponding RMS of the semiannual plus annual harmonic, suggesting the seasonal cycle as an important contributor to the total variability. Below 200 m depth, where semiannual and annual amplitudes are weak anyway, RMS of the residuals generally exceed the RMS of semiannual plus annual harmonic, indicating different time scales dominating the total variability.

While both mixed and upper thermocline layers undergo substantial fluctuations of potential temperature and salinity, the central water layer below remains rather stable on seasonal time scales (Figure 7a). At ~11°S, it is composed solely of South Atlantic Central Water (SACW, as defined in *Mohrholz et al.* [2008]), clearly distinguishable from the colder and fresher Eastern SACW (ESACW), which stems from the Benguela upwelling region. By investigating the seasonal cycle of salinity anomalies on isopycnals, substantial changes in the water mass contribution cannot be identified both for upper and lower limits of the central

water layer, represented by the 26.4 and 27.0 isopycnal, respectively (Figure 7b). Represented by the 25.8 isopycnal, seasonal salinity fluctuations in the upper thermocline are found in the range of ±0.05 with the annual component being dominant. These seasonal changes in water mass composition in the upper layers are attributed primarily to the annual cycle in surface heat and freshwater fluxes as well as river runoff, as meridional advection cannot account for the observed semiannual cycle of salinity due to rather small meridional advection length scales and weak meridional gradients of salinity on isopycnals.

4. Discussion and Conclusions

For the first time, multiyear observations off the coast of Angola are available to describe the eastern boundary circulation. Contrary to the conclusions drawn from historical synoptic measurements, no steady southward flow of the AC is observed at ~11°S off Angola. Instead, moored velocity time series of almost 2.5 years duration show strong intraseasonal variability with magnitudes in agreement with previous synoptic measurements [*Dias*, 1983a,1983b; *Mohrholz et al*., 2001; *Moroshkin et al*., 1970]. The mean southward alongshore velocity of the AC, however, does not exceed 8 cm/s. A corresponding boundary current transport time series is estimated based on the interpolation/extrapolation of the moored time series using variability patterns derived from a set of 13 shipboard velocity sections. A mean southward transport of 0.32 ± 0.046 Sv is found for the observation period. Semiannual and annual harmonics are both found to be important within the seasonal cycle having maximum southward transports during March/April and September/October. These periods approximately coincide with the passing times of the semiannual downwelling CTW [*Polo et al*., 2008; *Rouault*, 2012]. By poleward acceleration of the flow, this would result in the southward transport of warm, tropical waters [*Ostrowski et al*., 2009; *Rouault*, 2012]. It should be noted that the mooring observation period did not include a Benguela Niño or Niña, and can therefore be considered as a period with a rather regular seasonal cycle. Expectedly, the corresponding transport estimate from the mooring data is considerable smaller than the AC transport derived during the major Benguela Niño event in 1995 [*Mercier et al*., 2003].

Based on an extensive set of shipboard hydrographic data and autonomous glider measurements, the seasonality of potential temperature and salinity within the current regime is investigated. The main seasons of downwelling and upwelling in March and August, respectively, are well represented. Also, there are indications for a secondary upwelling in December/January, although this period is only sparsely sampled. The existence of the secondary upwelling was also evidenced in *Berrit and Dias* [1977], based on a 5 year temperature time series acquired at about 12°S on the shelf in 40 m water depth. Despite a considerable semiannual component in sea level anomalies at the mooring positions indicating the passage of upwelling CTWs in July/August and December/January, SST shows a strong cooling signal only during the major upwelling season in July/August, while only a minor cooling is observed during December/January (Figure 8). This dominance of the annual cycle relative to the semiannual cycle in near-surface temperature is most likely related to the annual cycle in surface heat fluxes. However, other processes like seasonal variations in diapycnal mixing might contribute. The upper 20–30 m are characterized by very fresh waters both in October/November and February/March/April. The freshening off the coast of Angola during austral summer has been previously associated with freshwater outflow from the Angolan rivers [*Mohrholz et al*., 2001]. Strength of Angolan river run-off is controlled by the wet season in the respective drainage areas. Run-off from the Congo and Cuanza rivers reaches its seasonal maximum in December/January (not shown, data for the Congo river published by *Dai et al*. [2009]). Yet, the timing of the freshening most likely is very sensitive to the yearly onset of the wet season. However, also the importance of year-to-year variability in rainfall over the adjacent landmasses and the study area itself must be considered. Revisiting the deep extension of the warm/fresh surface layer in October/November (Figure 6), we want to note that most of the data in this period stems from a single cruise/glider survey in 2015, when an anomalously strong downwelling was identified in

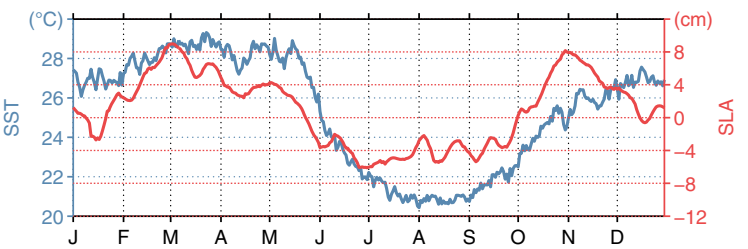

Figure 8. Seasonal cycle of SST (blue) and SLA (red) at ~11°S averaged over the mooring period (July 2013 to October 2015).

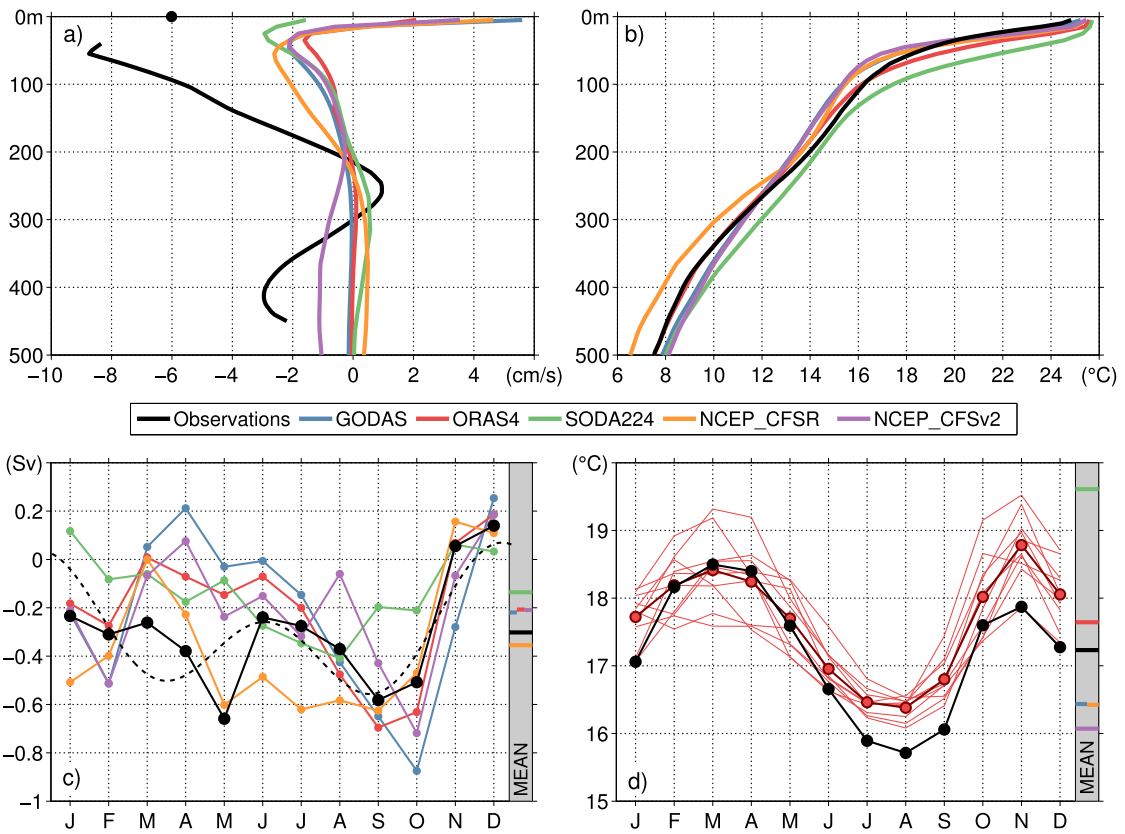

Figure 9. Profiles of (a) mean alongshore velocity and (b) potential temperature profiles from observations (black) and various reanalysis products (colors). Seasonal cycle of Angola Current transport from observations (black solid) and reanalysis products (colors) is shown in (c). Black-dashed line shows the sum of semiannual and annual harmonics from Figure 5b). Total mean AC transport values are indicated to the right. In (d) the mean seasonal cycle of potential temperature averaged over 50–100 m depth is shown for observations (black) and ORAS4 reanalysis (red). Thin red lines correspond to seasonal cycles derived from individual 2 year segments, while the bold red line shows the mean seasonal cycle derived from the total time series (1995–2014). Corresponding layer-averaged total mean values for both observations and reanalysis products are indicated to the right.

SLA data (SLA amplitude of ∼17 cm versus 8 cm in the climatology, not shown), most likely associated with the anomalous deepening of the isopycnals.

In order to identify seasonal changes in water mass composition, the mean seasonal cycle of salinity anomalies on selected isopycnals is investigated. Both lateral and vertical mixing as well as meridional advection by the AC are potential impact factors for water mass anomalies in the region. However, below the mixed layer, water mass characteristics appear to be primarily controlled by the annual cycle of surface heat and freshwater fluxes associated with vertical mixing. In particular, no clear connection between water mass composition and the semiannual component of the AC transport can be established. By contrast, in the northern Benguela a seasonal cycle of the central water characteristics is observed, coupled to the seasonality in the alongshore currents and meridional shift of the ABF [*Mohrholz et al.*, 2008]. However, at ∼11°S below the near-surface layer, alongshore gradients of hydrographic properties on isopycnals within the AC core are weak and seasonal alongshore advection length scales are small. More specifically, at the AC core depth, the semiannual harmonic amplitude of alongshore velocity that dominates the seasonal variability is 4.5 cm/s resulting in an advection length scale smaller than ±1°lat. With the isopycnal alongshore gradients of 0.045°C/°lat for temperature and 0.015/°lat for salinity, it is obvious that the alongshore advection associated with the seasonal cycle of the AC cannot induce a significant seasonality in water mass composition. The central water layer is composed almost purely of SACW with no seasonal influences by ESACW being identifiable, the latter originating in the Cape Basin.

Most coupled climate simulations exhibit warm SST biases in the coastal upwelling regions of the tropical Southeast Atlantic Ocean [*Davey et al.*, 2002; *Richter et al.*, 2014], particularly strong near the ABF region.

While mainly deficiencies in the atmospheric component have been suspected as source of the bias, *Xu et al.* [2014] argue that systematic errors in the ocean models are at least partly responsible for the biases seen in the coupled simulations. Poorly simulated subsurface thermal structures off Angola in combination with an overshooting AC near the ABF have been identified to cause erroneous southward advection of too-warm subsurface waters that are subsequently upwelled causing a warm SST bias in the northern Benguela. Nevertheless, a lack of in situ ocean observations within the boundary circulation and particularly the highly variable frontal region hampers a better understanding of the oceanic contribution to the biases in the region. The data sets presented in this study provide the opportunity for a first assessment of the performance of ocean reanalysis products upstream of the frontal region. Using the monthly output of five publically available reanalysis products (GODAS: 1995–2015, ORAS4: 1995–2014, SODA 2.2.4: 1995–2010, NCEP-CFSR: 1995–2010, NCEP-CFSv2: 2011–2015), we compare observed and simulated alongshore flow, AC transport, and temperature at the mooring array position at ∼11°S (Figure 9). The reanalysis products agree in showing a weak mean southward current of 1–3 cm/s at the AC core depth in about 50 m depth (Figure 9a). However, it should be noted that by confronting these values with observations, point measurements are compared to model results obtained at a horizontal resolution in the range of 0.5°–1°. Therefore, the AC transport estimates from the reanalysis products are based on one or two grid points only. Nevertheless, the mean AC transports from the reanalysis products and observations are similar (Figure 9c), indicating that the simulated velocity at the model grid points correspond to the observed section mean velocity rather than the observed velocity at the mooring position. Regarding AC transport seasonality, most of the products reproduce the southward transport maximum in September/October as well as the subsequent decrease, while the second southward maximum in May is generally not captured. Note, that the observed seasonal cycle based on climatological monthly means shows a southward transport maximum in May, while the sum of semiannual and annual harmonics (from Figure 5b) suggests a secondary transport maximum in March/April (black solid versus black-dashed line in Figure 9c). This underlines the uncertainty in the estimation of the mean seasonal cycle from the relatively short mooring time series due to the presence of strong intraseasonal fluctuations (Figure 5b). Only SODA 2.2.4 clearly reveals an erroneous downward displacement and weakened thermocline, while mean temperatures in GODAS, NCEP-CFSR, and NCEP-CFSv2 tend to be too cold in the AC depth range (Figure 9b). Note that all products show too warm near-surface temperatures, suggesting local warm SST biases. In terms of thermal structure ORAS4 appears to be closest to the observations, although showing also a slight downward displacement of the thermocline compared to our observations. The seasonal cycle of potential temperature averaged over the AC core range (50–100 m depth) indicates warm biases mainly during the upwelling seasons in ORAS4 (Figure 9d), whereas cold biases in NCEP-CFSR and NCEP-CFSv2 result mainly from a misrepresentation of the major downwelling season in austral autumn (not shown).

There is no indication of a strongly biased thermal structure at ∼11°S in ocean reanalysis products. When comparing observed and simulated alongshore velocities, one has to consider the relatively low horizontal model resolution. Mean velocity profiles from the reanalysis products generally reproduce the observed vertical structure, yet with smaller amplitudes. The simulated velocities correspond rather to the observed section-averaged velocity than to the velocity observed at the mooring with the observed and simulated mean AC transports being similar. However, near the ABF an intensification and overshooting of the AC in similar reanalysis products is described that displaces the front southward and advects warm subsurface water into the northern Benguela [*Xu et al.*, 2014]. If there is a local intensification of the AC near the ABF, it appears to be decoupled from the flow further upstream. Observations of processes in the frontal region contributing to cross-frontal exchange are crucial to improve our understanding of the origin of the bias in ocean simulations.

Acknowledgments

This study was supported by the German Federal Ministry of Education and Research as part of the SACUS project (03G0837A), and by European Union 7th Framework Programme (FP7 2007–2013) under grant agreement 603521 PREFACE project. Part of the CTD and shipboard ADCP data were acquired within the monitoring component of the Nansen Program, in cooperation with the Instituto Nacional de Investigação Pesqueira (INIP) in Angola, and were funded by the Norwegian Agency for Development Cooperation (Norad). We thank Volker Mohrholz for providing CTD profiles collected during three cruises carried out by the Leibniz Institute for Baltic Sea Research Warnemünde (IOW). Data sets described in sections 2.1 and 2.2 are available through https://doi.pangaea.de/10.1594/PANGAEA.868684. The altimeter data were produced by SSALTO/DUACS and distributed by AVISO with support from CNES (http://www.aviso.fr/duacs/). Microwave OI SST data are produced by Remote Sensing Systems and sponsored by National Oceanographic Partnership Program (NOPP) and the NASA Earth Science Physical Oceanography Program. Data are available at http://www.remss.com. GODAS data are provided by the NOAA/OAR/ESRL PSD, Boulder, Colorado, USA, from their web site at http://www.esrl.noaa.gov/psd/. ECMWF ORAS4 reanalysis data are available via ftp://ftp.icdc.zmaw.de/EASYInit/ORA-S4/. The CFSR and CFSv2 data were developed by NOAA's National Centers for Environmental Prediction (NCEP). Data can be accessed via http://rda.ucar.edu under data set number ds093.2 and ds094.2, respectively. SODA 2.2.4 was accessed via http://apdrc.soest.hawaii.edu/datadoc/soda_2.2.4.php. For glider and shipboard data processing the authors thank Gerd Krahmann. We thank the captains and crew of the RV Meteor as well as our technical group for their help with the fieldwork.

References

Bachèlery, M.-L., S. Illig, and I. Dadou (2016), Interannual variability in the South-East Atlantic Ocean, focusing on the Benguela Upwelling System: Remote versus local forcing, *J. Geophys. Res. Oceans*, *121*, 284–310, doi:10.1002/2015JC011168.

Barnett, T. P. (1983), Interaction of the monsoon and Pacific trade wind system at interannual time scales Part I: The equatorial zone, *Mon. Weather Rev.*, *111*(4), 756–773, doi:10.1175/1520-0493(1983)111 < 0756:IOTMAP > 2.0.CO;2.

Berrit, G. R., and C. A. Dias (1977), Hydroclimatologie des Régions Côtières de L'Angola, *Cah. Océanogr.*, *15*, 181–196.

Brandt, P., A. Funk, A. Tantet, W. Johns, and J. Fischer (2014), The equatorial undercurrent in the central Atlantic and its relation to tropical Atlantic variability, *Clim. Dyn.*, *43*(11), 2985–2997, doi:10.1007/s00382-014-2061-4.

Carr, M.-E., and E. J. Kearns (2003), Production regimes in four Eastern Boundary Current systems, *Deep Sea Res. Part II*, *50*(22–26), 3199–3221, doi:10.1016/j.dsr2.2003.07.015.

Chavez, F. P., and M. Messié (2009), A comparison of Eastern Boundary Upwelling Ecosystems, *Prog. Oceanogr.*, *83*(1–4), 80–96, doi:10.1016/j.pocean.2009.07.032.
Dai, A., T. Qian, K. E. Trenberth, and J. D. Milliman (2009), Changes in continental freshwater discharge from 1948-2004, *J. Clim.*, *22*, 2773–2791, doi:10.1175/2008JCLI2592.1.
Davey, M., et al. (2002), STOIC: A study of coupled model climatology and variability in tropical ocean regions, *Clim. Dyn.*, *18*(5), 403–420, doi:10.1007/s00382-001-0188-6.
Dias, C. A. (1983a), Note on the evidence of a permanent southward flow of the upper oceanic tropospheric waters off Angola at 12°S, *Collect. Sci. Pap. Int. Comm. Southeast Atlantic Fish.*, *10*, 99–102.
Dias, C. A. (1983b), Preliminary report on the physical oceanography off southern Angola, March and July 1971, *Collect. Sci. Pap. Int. Comm. Southeast Atlantic Fish.*, *10*, 103–116.
Durgadoo, J. V., B. R. Loveday, C. J. C. Reason, P. Penven, and A. Biastoch (2013), Agulhas leakage predominantly responds to the southern hemisphere westerlies, *J. Phys. Oceanogr.*, *43*(10), 2113–2131, doi:10.1175/JPO-D-13-047.1.
Florenchie, P., J. R. E. Lutjeharms, C. J. C. Reason, S. Masson, and M. Rouault (2003), The source of Benguela Niños in the South Atlantic Ocean, *Geophys. Res. Lett.*, *30*(10), 1505, doi:10.1029/2003GL017172.
Gammelsrød, T., C. H. Bartholomae, D. C. Boyer, V. L. L. Filipe, and M. J. O'Toole (1998), Intrusion of warm surface water along the Angolan-Namibian coast in February–March 1995: The 1995 Benguela Nino, *S. Afr. J. Mar. Sci.*, *19*(1), 41–56, doi:10.2989/025776198784126719.
Grodsky, S. A., J. A. Carton, S. Nigam, and Y. M. Okumura (2012), Tropical Atlantic Biases in CCSM4, *J. Clim.*, *25*(11), 3684–3701, doi:10.1175/JCLI-D-11-00315.1.
Harlaß, J., M. Latif, and W. Park (2015), Improving climate model simulation of tropical atlantic sea surface temperature: The importance of enhanced vertical atmosphere model resolution, *Geophys. Res. Lett.*, *42*, 2401–2408, doi:10.1002/2015GL063310.
Huang, B., Z.-Z. Hu, and B. Jha (2007), Evolution of model systematic errors in the Tropical Atlantic Basin from coupled climate hindcasts, *Clim. Dyn.*, *28*(7), 661–682, doi:10.1007/s00382-006-0223-8.
Kostianoy, A. G., and J. R. E. Lutjeharms (1999), Atmospheric effects in the Angola-Benguela frontal zone, *J. Geophys. Res.*, *104*(C9), 20,963–20,970, doi:10.1029/1999JC900017.
Large, W. G., and G. Danabasoglu (2006), Attribution and impacts of upper-ocean biases in CCSM3, *J Clim.*, *19*(11), 2325–2346, doi:10.1175/JCLI3740.1.
Lübbecke, J. F., C. W. Böning, N. S. Keenlyside, and S.-P. Xie (2010), On the connection between Benguela and equatorial Atlantic Niños and the role of the South Atlantic Anticyclone, *J. Geophys. Res.*, *115*, C09015, doi:10.1029/2009JC005964.
Meeuwis, J. M., and J. R. E. Lutjeharms (1990), Surface thermal characteristics of the Angola-Benguela front, *S. Afr. J. Mar. Sci.*, *9*(1), 261–279, doi:10.2989/025776190784378772.
Mercier, H., M. Arhan, and J. R. E. Lutjeharms (2003), Upper-layer circulation in the eastern Equatorial and South Atlantic Ocean in January–March 1995, *Deep Sea Res., Part I*, *50*(7), 863–887, doi:10.1016/S0967-0637(03)00071-2.
Mohrholz, V., M. Schmidt, and J. R. E. Lutjeharms (2001), The hydrography and dynamics of the Angola-Benguela Frontal Zone and environment in April 1999, *S. Afr. J. Sci.*, *97*(May/June 2001), 199–208.
Mohrholz, V., C. H. Bartholomae, A. K. van der Plas, and H. U. Lass (2008), The seasonal variability of the northern Benguela undercurrent and its relation to the oxygen budget on the shelf, *Cont. Shelf Res.*, *28*(3), 424–441, doi:10.1016/j.csr.2007.10.001.
Mohrholz, V., A. Eggert, T. Junker, G. Nausch, T. Ohde, and M. Schmidt (2014), Cross shelf hydrographic and hydrochemical conditions and their short term variability at the northern Benguela during a normal upwelling season, *J. Mar. Syst.*, *401*, Part B, 92–110, doi:10.1016/j.jmarsys.2014.04.019.
Moroshkin, K. V., V. A. Bunov, and R. P. Bulatov (1970), Water circulation in the eastern South Atlantic Ocean, *Oceanology*, *10*, 27–34.
Ostrowski, M., J. C. B. da Silva, and B. Bazik-Sangolay (2009), The response of sound scatterers to El Niño- and La Niña-like oceanographic regimes in the southeastern Atlantic, *ICES J. Mar. Sci.*, *66*(6), 1063–1072, doi:10.1093/icesjms/fsp102.
Patricola, C. M., M. Li, Z. Xu, P. Chang, R. Saravanan, and J.-S. Hsieh (2012), An investigation of tropical Atlantic bias in a high-resolution coupled regional climate model, *Clim. Dyn.*, *39*(9), 2443–2463, doi:10.1007/s00382-012-1320-5.
Peterson, R. G., and L. Stramma (1991), Upper-level circulation in the South Atlantic Ocean, *Prog. Oceanogr.*, *26*(1), 1–73, doi:10.1016/0079-6611(91)90006-8.
Polo, I., A. Lazar, B. Rodriguez-Fonseca, and S. Arnault (2008), Oceanic Kelvin waves and tropical Atlantic intraseasonal variability: 1. Kelvin wave characterization, *J. Geophys. Res.*, *113*, C07009, doi:10.1029/2007JC004495.
Pujol, M. I., Y. Faugère, G. Taburet, S. Dupuy, C. Pelloquin, M. Ablain, and N. Picot (2016), DUACS DT2014: The new multi-mission altimeter data set reprocessed over 20 years, *Ocean Sci.*, *12*(5), 1067–1090, doi:10.5194/os-12-1067-2016.
Richter, I., and S.-P. Xie (2008), On the origin of equatorial Atlantic biases in coupled general circulation models, *Clim. Dyn.*, *31*(5), 587–598, doi:10.1007/s00382-008-0364-z.
Richter, I., S. K. Behera, Y. Masumoto, B. Taguchi, N. Komori, and T. Yamagata (2010), On the triggering of Benguela Niños: Remote equatorial versus local influences, *Geophys. Res. Lett.*, *37*, L20604, doi:10.1029/2010GL044461.
Richter, I., S.-P. Xie, S. K. Behera, T. Doi, and Y. Masumoto (2014), Equatorial Atlantic variability and its relation to mean state biases in CMIP5, *Clim. Dyn.*, *42*(1), 171–188, doi:10.1007/s00382-012-1624-5.
Rouault, M. (2012), Bi-annual intrusion of tropical water in the northern Benguela upwelling, *Geophys. Res. Lett.*, *39*, L12606, doi:10.1029/2012GL052099.
Rouault, M., P. Florenchie, N. Fauchereau, and C. J. C. Reason (2003), South East tropical Atlantic warm events and southern African rainfall, *Geophys. Res. Lett.*, *30*(5), 8009, doi:10.1029/2002GL014840.
Rouault, M., S. Illig, C. Bartholomae, C. J. C. Reason, and A. Bentamy (2007), Propagation and origin of warm anomalies in the Angola Benguela upwelling system in 2001, *J. Mar. Syst.*, *68*(3–4), 473–488, doi:10.1016/j.jmarsys.2006.11.010.
Schmidtko, S., G. C. Johnson, and J. M. Lyman (2013), MIMOC: A global monthly isopycnal upper-ocean climatology with mixed layers, *J. Geophys. Res. Oceans*, *118*, 1658–1672, doi:10.1002/jgrc.20122.
Shannon, L. V., A. J. Boyd, G. B. Brundrit, and J. Taunton-Clark (1986), On the existence of an El Niño-type phenomenon in the Benguela System, *J. Mar. Res.*, *44*(3), 495–520, doi:10.1357/002224086788403105.
Thomsen, S., T. Kanzow, G. Krahmann, R. J. Greatbatch, M. Dengler, and G. Lavik (2016), The formation of a subsurface anticyclonic eddy in the Peru-Chile Undercurrent and its impact on the near-coastal salinity, oxygen, and nutrient distributions, *J. Geophys. Res. Oceans*, *121*, 476–501, doi:10.1002/2015JC010878.
Wacongne, S., and B. Piton (1992), The near-surface circulation in the northeastern corner of the South Atlantic ocean, *Deep Sea Res., Part A*, *39*(7–8), 1273–1298, doi:10.1016/0198-0149(92)90069-6.
Xu, Z., M. Li, C. M. Patricola, and P. Chang (2014), Oceanic origin of southeast tropical Atlantic biases, *Clim. Dyn.*, *43*(11), 2915–2930, doi:10.1007/s00382-013-1901-y.